Pacific Decadal Oscillation and recent oxygen decline in the eastern tropical Pacific Ocean

Olaf Duteil[1], Andreas Oschlies[1] , Claus W. Böning[1]

[1] GEOMAR – Helmholtz Centre for Ocean Research Kiel, Düsternbrooker Weg. 20, 24103 Kiel, Germany

Correspondence to **:** Olaf Duteil (oduteil@geomar.de)

Abstract

The impact of the positive and negative phases of the Pacific Decadal Oscillation (PDO) on the extension of the poorly oxygenated regions of the eastern Pacific Ocean has been assessed using a coupled ocean circulation-biogeochemical model. We show that during a "typical" PDO-positive phase the volume of the suboxic regions expands by 7 % in 50 years due to a slow-down of the large-scale circulation related to the decrease of the intensity of the trade winds. Changes in oxygen levels are mostly controlled by advective processes between 10°N and 10°S while the diffusive processes are dominant poleward of 10°: in a "typical" PDO-positive phase the sluggish equatorial current system provides less oxygen into the eastern equatorial part of the basin while the oxygen transport by diffusive processes significantly decreases south of 10°S. The suboxic region located north of 10°N displays less sensitivity to the phase of the PDO as the local upwelling-related processes play a dominant role compared to the large-scale circulation in setting the oxygen concentration. Our study suggests that the prevailing PDO-positive conditions since 1975 may explain a significant part of the current deoxygenation occurring in the eastern Pacific Ocean.

1. Introduction

Oxygen is one of the most important chemical elements in the ocean, as marine organisms ranging from microorganisms to vertebrates use it for respiration. Its concentration is regulated both by circulation and by biogeochemical processes. In general, high-latitude regions are characterized by high oxygen concentrations, while subsurface tropical regions are poorly oxygenated. Particularly in the eastern parts of the tropical oceans, the large export of organic material out of productive surface layers combined with the sluggish circulation depletes oxygen levels at depth, resulting in the formation of large suboxic regions where the oxygen concentration falls below 20 $mmol.m^{-3}$ (Karstensen et al., 2008). The overall contrast between high latitudes and tropical shadow zones is generally well reproduced by ocean models (Bopp et al., 2013; Cocco et al., 2013, Cabré et al., 2015, Shigemitsu et al., 2017).

The temporal variability of oxygen concentrations in the ocean interior is nevertheless still poorly understood, in particular in the eastern tropical Pacific Ocean, where oxygen concentrations are among the lowest worldwide (Karstensen et al., 2008). A strong decrease of oxygen concentrations in these regions has been inferred from observations from the 1960s to the 2000s (Stramma et al., 2008, 2012; Schmidtko et al., 2017). This deoxygenation is not correctly reproduced by current ocean models (Oschlies et al., 2017). It is not clear whether the changes in oxygen concentration are due to anthropogenic changes (Matear et al., 2003; Long et al., 2016, Ito et al., 2017), or are related to natural low-frequency climate oscillations such as the Pacific Decadal Oscillation (PDO) (Deutsch et al., 2014), a robust and recurring pattern of ocean atmosphere climate variability centered over the mid-latitude north Pacific basin (Mantua et al., 1997).

The stronger trade winds occurring during a negative phase of the PDO cause a shoaling of the eastern thermocline of the tropical and subtropical Pacific Ocean (Miller et al., 1994) (see the Supplementary Figure 1 for an overview of the mechanisms controlling the oxyen levels in the eastern tropical ocean). Deutsch et al. (2011, 2014) showed that the

depth of the thermocline regulates the oxygen levels in the north eastern subtropical Pacific Ocean. In these regions, a shallower thermocline fosters low oxygen concentrations in the intermediate ocean as a larger amount of organic material is respired below the mixed layer (Deutsch et al., 2011). Simultaneously, in the tropical regions the zonal volume transport by the equatorial current system increases during a negative PDO event as does the meridional transport by the sub-tropical cells (STCs) (Hong et al., 2014), which connect the subtropics to the tropics (McCreary and Lu, 1994). The variability of the strength of the STCs forces the variability of the oxygen transport in the upper thermocline of the equatorial Pacific Ocean (Duteil et al., 2014a). A competition takes place between the increased oxygen transport and the increased respiration as primary production is enhanced by the increased nutrient supply. Finally, stronger trade winds also increase the subduction volume of the North (Qu et al., 2009) and South Pacific Eastern Subtropical Mode Waters (Luo et al., 2011). A subtropical increase of productivity related to an increase of the trade winds causes a negative oxygen anomaly in these mode waters, which is transported equatorward and leads to a delayed oxygen decrease in tropical regions as shown by Ridder and England (2014) in an Earth System Model of intermediate complexity.

All these studies highlight the potential effect of the PDO on oxygen concentrations and show that the processes at play are diverse and strongly region dependent. However, we still do not have a clear picture of the impact of the PDO on the suboxic regions and on the oxygen levels of the eastern Pacific Ocean. Indeed, the studies cited above focus either specifically on the suboxic regions of the north eastern Pacific region (Deutsch et al., 2011, 2014) or on the upper thermocline of the tropical Pacific Ocean (Duteil et al., 2014a). A caveat of the model used by Ridder and England (2014) is that the equatorial undercurrent (EUC) is represented poorly, as is the case for most coarse-resolution (lower than 0.5° at the equator) models (Karnauskas et al., 2012). The EUC indeed ventilates the suboxic regions, as shown by Cabre et al. (2015), Shigemitsu et al. (2017) in a range of models part of the Coupled Model Intercomparison Project 5 (CMIP5).

Understanding precisely the role of the PDO in setting oxygen levels is difficult in “traditional” 50-years hindcasts experiments (Deutsch et al.,2011; Ito et al., 2013; Duteil et al., 2014) due to the superposition of a long-term climate trend and higher-frequency climate oscillations such as the El Nino Southern Oscillation (ENSO) (Ito et al., 2013, 2016; Eddebbar et al., 2017). Ito et al. (2013) showed that the temporal spectrum of oxygen concentrations of the north eastern tropical Pacific Ocean is characterized by a strong decadal variance which may partly arise from the ‘reddening’ of the variability spectrum of the physical and biological drivers (Ito and Deutsch, 2010), suggesting, e.g. a contribution of ENSO to the decadal oxygen variability, in complement to the PDO.

Rather than performing a “hindcast” experiment, we here specifically isolate and assess the role of the phase of the PDO on the oxygen levels of the tropical eastern Pacific Ocean by forcing a coupled circulation – biogeochemical model using “typical” conditions characteristic of the negative and positive PDO phases. These idealised atmospheric forcings are derived from monthly averages of realistic winds and heat fluxes of the 1948 – 2007 COREv2 dataset (Large and Yeager, 2009). Our aim is to understand whether and by which processes (oxygen advection, diffusion, respiration) the PDO may be responsible of the observed oxygen decline in the suboxic regions of the tropical eastern Pacific Ocean.

This paper is organized as follows. The section 2 describes the construction of the “typical” PDO forcings and the configuration of the experiments that we perform. In section 3, we assess the basin-scale circulation of our experiments. In section 4, we present the difference in oxygen levels between a “typical” positive and negative PDO phase. The mechanisms regulating the oxygen levels are described in section 5. Temporal aspects are discussed in Section 6. In

section 7 we discuss the changes in the upwelling systems and the impact on suboxia. We summarize our results in section 8.

2. Forcings and experiments

The NEMO ocean model version v3.6 (Madec et al., 2008) has been used in the standard configuration ORCA2. This configuration has been widely used in previous studies and constitutes the ocean component of the ISPL-CM5A model, part of the Coupled Model Intercomparison Project (CMIP5) effort (Dufresnes et al., 2013). Its zonal resolution is 2 degrees. The mean meridional resolution is 2 degrees outside the tropics and increases to 0.5 degrees close to the equator. The resolution of ORCA2 is sufficient to realistically reproduce the EUC (Cravatte et al., 2007) and the subtropics - tropics connectivity (Luebbecke et al., 2008). The circulation model has been coupled to a 6-compartments (nutrient, phytoplankton, zooplankton, particulates and dissolved detritus, oxygen) biogeochemical model . This model is described in detail in Kriest et al. (2010). It has been adapted by Duteil et al. (2014a,b) to the NEMO framework.

We constructed 3 atmospheric forcing datasets derived from the interannual 1948 – 2007 COREv2, 6h temporal resolution, forcing dataset (Large and Yeager, 2009):

- MEAN : 1- A low-pass filter has been applied to remove the frequencies with a period shorter than 1 month. 2- The long term trend 1948 – 2007 (Yang et al., 2016) has been removed. 3- The corresponding time steps of the individual annual forcings of the year 1948 – 2007 have been averaged to reconstruct a climatological annually cycling forcing set. The difference between MEAN and the COREv2 “normal year” is the absence of high frequency variability (< 1 month) and the removal of the long term trend implicitly contained in the “normal year”.
- PDO_PLUS (PDO_MINUS) : the steps 1- and 2- are similar as above. In PDO_PLUS (PDO_MINUS), the corresponding time step of the years characterized by a positive (negative) PDO phase (Fig. 1a) have been averaged, leading to the reconstruction of a 1 year, 6h temporal resolution, climatological forcing “typical” of a PDO-positive (negative) phase.

In PDO_PLUS the zonal wind speed decreases by about 0.2 to 0.5 ms^{-1} compared to MEAN in the mid-equatorial Pacific Ocean, where the winds are strongest (at least 8 ms^{-1}) (Fig. 1b). It increases close to the eastern coast by up to 0.3 ms^{-1}, where the winds are weaker (2 to 8 ms^{-1}). A similar pattern has been described by Merrifield et al. (2012) and Zhou et al. (2017). The meridional wind speed decreases by about 0.2 ms^{-1} (Fig. 1c). The 10 m air temperature increases by 0.1 to 0.3 °C in the eastern Pacific Ocean and decreases in the gyres (Fig. 1d). PDO_MINUS presents the opposite pattern.

We spin up the model during 1000 years using the forcing dataset MEAN. We subsequently performed 2 experiments using the forcing datasets PDO_PLUS and PDO_MINUS, respectively, that we integrate for a period of 50 years, which corresponds to the typical oscillation period of the PDO during the past 200 years (Mc Donald and Case, 2005).

3. Basin scale circulation

3.1. Gyres

The subtropical gyres (STG) slow down and extends equatorward in PDO_PLUS, constraining the tropical gyres (TG) (Fig 1e). The slow-down reaches up to 5 Sv (or 5-10 %). These results are consistent with the ones of Messie and Chavez (2011): analyzing the variability of the Extended Reconstruction Sea Surface Temperature (1910 – 2010) product (Smith et al., 2003), they show that the intensity of the northern and southern Pacific subtropical gyre decreases during a positive PDO event (their Fig. 10). The thermocline depth shoals in PDO_PLUS in the STG and deepens in

the eastern tropical part of the basin, correlated with a rise in sea level (Fig 1f). The large signal observed at 10°N is related to the extension of the STG. The passive adjustment time of the ocean (without considering ocean atmosphere feedbacks) is quick (a few years), which is coherent with previous studies (Zhang and Delworth, 2015; Deser et al., 1999; Hong et al., 2014).

3.2. Meridional overturning

The shallow meridional overturning is characterized by the presence of the STCs (Fig 1g). These cells are shallow (upper 500 m meters) structures connecting the subtropics and tropical regions (McCreary and Lu, 1994) and respond to a change in wind stress by baroclinic adjustment (Hong et al., 2014). The strength of the STCs (and therefore of the whole tropical current system, including the equatorial upwelling and the equatorial undercurrent) decreases by up to 5 Sv (10%) in PDO_PLUS compared to PDO_MINUS. The order of magnitude of the strength of the STCs in the PDO_PLUS and PDO_MINUS experiments are in line with other modeling studies (Lohman and Latif, 2005; Luebbecke et al., 2008; Hong et al., 2014) and with the observational study of McPhaden and Zhang (2002), who showed that the equatorial upwelling decreased by 10 % from 1970-77 (47 Sv) to 1980-89 (42 Sv) related with a shift of the phase of the PDO.

4. Oxygen concentration

4.1. Comparison with the World Ocean Atlas

At the end of the spinup, the model reproduces the large-scale features of the observed World Ocean Atlas (WOA) (Garcia et al., 2013) oxygen concentration field (Fig. 2a). The thickness of the SUB20 regions, defined as the regions where oxygen concentrations are lower than 20 $mmol.m^{-3}$ at the end of the spinup, reaches more than 700 m north of the equator both in the WOA (Fig. 2b) and in the model (Fig. 2c). 'Typical' biases (Bopp et al., 2013; Cabre et al., 2015) are present in our model. In particular: 1- the OMZ region does not extend far enough westward, in particular north of the equator, 2- oxygen concentrations at the equator are too low, maybe due to a poor representation of the intermediate current system, located below the EUC, in relatively coarse resolution models (Marin et al., 2010; Getzlaff and Dietze, 2013). The thickness of the suboxic regions is nevertheless lower in the equatorial region compared to the tropics, as shown in Fig. 2c

4.2. Perturbation by the PDO

After 50 years of integration, the oxygen (average 100 – 700 m) concentration is lower in the eastern part of the basin in PDO_PLUS compared to PDO_MINUS (Fig. 2d). This decrease reaches up to 100 % in regions where the oxygen is very low (below 5 $mmol.m^{-3}$) and about 5-10 % in regions where the oxygen concentration is lower than about 20 $mmol.m^{-3}$ (Fig. 2e). The volume of the SUB20 regions is larger by 7 % in PDO_PLUS and the thickness of the suboxic layer increases by up to 100 m close to the coast between 10°N and 10°S and at the outer boundary of the SUB20 regions (Fig. 2f) (note that the "stepwise shape" of the anomaly is due to the discretization of the vertical grid of the ocean model). The oxygen concentration in the SUB20 regions decreases by 2-10 $mmol.m^{-3}$ in PDO_PLUS compared to PDO_MINUS (0.04 to 0.2 $mmol.m^{-3}.yr^{-1}$). Conversely, in the mid-Pacific Ocean oxygen concentrations are larger in PDO_PLUS by 2 to 20 %. This increase is localized (5-10°N and 5-10°S and eastward of 160°W).

Our results can be put in perspective with observations. An oxygen decrease by 1 $mmol.m^{-3}yr^{-1}$ has been monitored in the eastern equatorial region (85°W, 2°S to 8°S) since 1976 (Czeschel et al., 2012). Schmidtko et al. (2017) found a global decrease of the integrated oxygen concentration in the water column since 1960. This decrease is of the order of 0.2 $mmol.m^{-3}yr^{-1}$ in the equatorial Pacific Ocean at 300 m depth. Similarly, Ito et al. (2017) shows that oxygen declines

at 400 m depth by 0.2 mmol.m^{-3} .yr^{-1} since 1958 in the eastern Pacific Ocean; at 100 m depth, oxygen decreases by up to 0.4 mmol.m^{-3}yr^{-1} . They, however, observed a localized oxygen increase at 10°N, similar to the one that we described above. Our simulations suggest that a shift from a negative to a positive phase of the PDO may be responsible for a large fraction of the observed oxygen decrease.

5. Regulation of the oxygen levels

The oxygen level below the euphotic zone is determined by the balance between consumption (respiration) and supply (transport). The supply is decomposed into advective, diapycnal and isopycnal diffusion terms. The analysis is based on the average of the 50 years of integration.

5.1. Intermediate (100 – 700m) tropical Pacific Ocean

The respiration processes remove oxygen (Fig. 3a), especially in the tropical regions (up to 10mmol.m^{-3}yr^{-1} in the layer 100-700 m), as the biological production is high along the equator and close to the coast. In the experiment PDO_PLUS the basin-scale circulation is more sluggish than in PDO_MINUS (See 3. 'Basin Scale Circulation'), leading to a decrease of the concentration of nutrients in the euphotic zone (see '7. Productivity and Upwellings'). The respiration term becomes "less negative" in PDO_PLUS (positive anomaly of 1-2 mmol.m^{-3} yr^{-1} in the equatorial region - Fig. 2d).

The consumption of oxygen is compensated by supply processes (Fig. 3b), partly performed by advective processes (Fig. 3c) which dominate the supply between 5°N and 5°S and in the eastern part of the basin, showing the preponderant role of the equatorial current system to supply oxygen to the oxygen-depleted regions (Cabre et al., 2015; Shigemitsu et al., 2017). Conversely, the diffusive processes (isopycnal and diapycnal mixing) dominate the supply outside of the equatorial region (poleward of 10°). (Fig. 3d). The ocean currents shape the thermocline and high oxygen concentrations are transferred by isopycnal diffusion from the core of the EUC to the poleward intermediate ocean. The PDO_PLUS – PDO_MINUS positive oxygen anomaly in the western part of the basin is caused by the decrease of the respiration ("less negative" values), which is not completely compensated by the decrease of the supply terms.

5.2. SUB20 regions

The contribution of each process has been vertically and zonally averaged over the SUB20 region of the Pacific Ocean (Fig. 4a) and multiplied by the longitudinal extension of the SUB20 of the experiment PDO_MINUS. The total supply term (Fig. 4a - black) is characterized by a large supply in the equatorial region, between 10°N and 10°S, due to advective processes (Fig. 4a - red). The role of the westward South and North equatorial currents is clearly apparent at 5°N and 5°S. At this location the thermocline exhibits a strong slope with strong oxygen gradients, fostering isopycnal diffusion (Fig. 4a - blue), removing oxygen from the equator (and the EUC) and transferring it to the deeper, adjacent regions. The effect of the jets and the isopycnal diffusion are adding up and cause the strong peak in oxygen supply, located between 5°S and 10°S (and to a lesser extent between 5°N and 10°N). The role of the oxygen supply by diapycnal diffusion (Fig 4a. – green) is relatively small in the equatorial region (about 20% of the total supply), but more significant between 30°S and 10°S (about one third of the total supply) and dominant north of 10°N (Fig 4b). Between 10°S and 30°S, the isopycnal diffusion term (Fig. 4a – blue) plays a dominant role, possibly due the outcrop of isopycnals and the formation of mode waters close to the southern part of SUB20. The importance of the isopycnal diffusion in setting the oxygen levels in the region off Chile (around 30°S) has been previously highlighted by sensitivity tests to the Redi mixing coefficient (Gnanadesikan et al. 2012). Stramma et al. (2010) roughly estimated the oxygen budget (30°N – 30°S) in the suboxic regions based on observational data. Despite large uncertainties, the

observational budget estimate points to an allocation of about 33 % by advection, 22 % by vertical mixing and 45 % by eddy mixing (Brandt et al., 2015). In our model, averaging the SUB20 budget between 30°N and 30°S gives comparable magnitudes (Fig. 4b) (in PDO_MINUS: 21 % of the supply occurs by advection, 29 % by diapycnal mixing and 50 % by isopycnal mixing, strongly related with mesosocale activity).

In the experiment PDO_PLUS, the supply of oxygen by circulation processes decreases (Fig. 4c – black) due to a reduction of the advective supply in the equatorial region (Fig. 4d – red) and of the diapycnal and isopycnal diffusion poleward of 10°N and 10°S (Fig. 4d – blue and green). The primary production decreases as well, resulting in a positive anomaly of the respiration term (which is 'less negative') (Fig. 4c – green). The decrease of respiration nearly compensates the reduced supply of oxygen especially in the equatorial region: the decrease of the circulation supply terms is however larger, leading to a net decrease of oxygen levels in SUB20 (Fig. 4c – red). In the region 10°N-30°N, about half of the oxygen decrease is caused by changes of the supply, while the other half is due to changes in respiration, triggered by changes in the advective processes (see 7 'Productivity and upwelling'). In the region 10°S-30°S, the decrease of the oxygen levels is principally due to a decrease of the isopycnal and mixing processes (Fig. 4d). As the ocean circulation is generally weaker in PDO_PLUS, the relative importance of diffusion increases in the PDO_PLUS experiment compared to PDO_MINUS (20 % of the supply occurs by advection, 27 % by diapycnal mixing and 53 % by isopycnal mixing) (Fig. 4b)

6. Temporal aspects

6.1. Intermediate (100 – 700m) tropical Pacific Ocean

In the western part of the basin (160°E-140°W, 10°N-10°S), oxygen concentrations decrease in PDO_PLUS compared to PDO_MINUS in the first years of the experiment (initial shock, highlighting the time scale of response of productivity to a change in circulation) and increase afterwards (Fig 5.a-d). The changes in the advective processes (Fig 5e. - blue) are largely responsible for the total changes in the supply (Fig. 5e - bold black). The decrease in respiration (Fig 6e - green) offsets these changes, leading to net a positive anomaly (Fig 5e - bold red). After 50 years the positive anomaly is still growing but at a slower pace (Fig. 5a): diffusive processes (cyan) (and more specifically diapycnal diffusion (pink) act in the same direction as the currents-driven changes as a result of a less stratified upper ocean under PDO_PLUS conditions (while the PDO_PLUS surface fluxes warms the surface ocean and foster a strong upper ocean stratification, the PDO_PLUS winds weaken the upwelling, warm the subsurface ocean, and foster a weak upper ocean stratification. The latter effect overcompensates the surface warming and explains that the ocean is less stratified under PDO_PLUS conditions compared to PDO_MINUS)

6.2 SUB20 regions

The picture described above shows similarities with the one of the equatorial region (10°N-10°S) of SUB20, where a strong decrease of the oxygen supply (Fig. 5f – bold black) due to advective processes (Fig. 5f – blue) occurs. The role of diffusion (Fig. 5f – pink) is however larger in SUB20 compared to the mid Pacific equatorial region. Respiration changes (Fig. 5f – green) do not offset the weaker supply, as in the western tropical Pacific Ocean, leading to a net decrease of oxygen concentration (Fig 5a-d). In the northern part (10°N-30°N) of SUB20 an increase of oxygen transport by advective processes (Fig. 5g - blue) is compensated by a strong decrease by diffusion processes (less mixing), leading to a net decrease of oxygen supply. Primary production and respiration increases (see 7 'Productivity and upwelling'), reinforcing the decrease of oxygen levels. In the southern part (10°S-30°S) of SUB20 the decrease of the oxygen supply by advective transport (Fig 5h – blue) is accompanied by a strong decrease of supply by diapycnal (Fig. 6h – pink) and isopycnal mixing (Fig. 5h - cyan). The adjustment occurs on (multi) decadal time scale (Fig. 5a-d). The strong changes in the supply mechanisms in the northern / southern part of the SUB20 regions are likely linked to a

stronger influence of the subtropical regime in PDO_PLUS than in PDO_MINUS in SUB20 (see 3. 'Basin Scale Circulation'), which explains the 'initial shock' related with a change of regime.

The simulated PDO-induced changes are significant after at least 5 years (in the equatorial Pacific Ocean) to a few decades (in the southern part of the suboxic regions). Significant changes occurred after a similar time scale in the study of Ridder and England, 2014. It suggests that higher frequency climate oscillations such as the El Nino Southern Oscillation (ENSO) – or "short-lasting" PDO events - have a very limited impact on oxygen concentrations of the suboxic eastern tropical Pacific, in agreement with Deutsch et al. (2011) and Ito et al. (2013). ENSO may however have an impact on the surface air/sea oxygen exchanges (Eddebar et al., 2017) and "short-lasting" PDO events (less than 10 years) may impact the oxygen concentration of the upper thermocline of the mid-Pacific Ocean (Duteil et al., 2014b). In the southern region (10°S-30°S), the system is still losing oxygen after 50 years of integration suggesting that extra-tropical processes are involved. Getzlaff et al. (2016) showed that a vigorous South Pacific subtropical gyre, driven by an increases of the southern hemisphere westerlies, supplies oxygen to the tropics. Yamamoto et al. (2015), Keller et al. (2016) showed that high latitudes may constrain tropical suboxic regions at multi-decadal and centennial time scale.

7. Productivity and upwelling

As we have seen before the changes in respiration play a significant role in setting the oxygen levels. Respiration either compensates the changes in supply in the equatorial region or acts in synergy with the decrease in supply to deplete oxygen in the northern part of SUB20 in the PDO_PLUS experiment. While the changes in oxygen supply and transport are primarily linked to changes in the structure of the interior ocean, the change in respiration is primarily linked to the surface and upper thermocline productivity, which ultimately depends of the supply of nutrients to the mixed layer.

7.1. Upwelling strength and seasonality

In the PDO_PLUS experiment, the nutrient supply decreases over most of the basin, leading to a decrease of the nutrient uptake and the productivity. The decrease of the supply is caused both by a slowing-down of the circulation and by a thermocline deepening (as seen in 3. "Basin Scale Circulation"). However, counter intuitively, nutrient levels increase and the production is slightly (2-5%) higher in PDO_PLUS in the eastern upwelling systems. Fig. 6a presents similarities with the imprint of the PDO on deseasonalized chlorophyll concentration inferred from satellite data (Thomas et al., 2012). They found that a positive phase of the PDO is associated with a general decrease of chlorophyll concentration in the tropical Pacific Ocean. In the region located between 15°N-30°N and east of 140°W, and in the region south of 10°S and east of 120°W the correlation between PDO and deseasonalized chlorophyll is however positive (their figure 7). Furthermore, other climate oscillations, such as the North Pacific Gyre Oscillation (NPGO) constrain the strength of the upwelling cells in the ETNP in complement to the PDO (DiLorenzo et al., 2008; Macias et al., 2012).

The productivity increase in PDO_PLUS is due to change in seasonality of the upwelling system in our experiments. The Eastern Tropical South Pacific (ETSP) region (average 10°S-30°S, 90°W-60°W) is characterized by a strong downwelling in May / April and a strong upwelling in August / September in PDO_MINUS (Fig. 6c). Conversely, in PDO_PLUS, the ETSP is characterized by a weaker upwelling which albeit lasts during all year, continuously supplying nutrients into the ML and the upper ocean and creating a positive anomaly in nutrients and productivity (Fig 6e and Fig 6g). In the Eastern Tropical North Pacific (ETNP) (10°N-30°N, 120°W-90°W), a strong upwelling occurs one month earlier in PDO_PLUS than in in PDO_MINUS (Fig. 6d), leading to an increase in nutrient concentrations in the upper ocean (Fig. 6f and Fig. 6h) in a season where irradiance is high, fostering primary production. The positive

PDO years used to construct the PDO_PLUS forcing are constituted by 30 % of positive NPGO years, which may explain the shift in the upwelling seasonality and the stimulation of productivity in the ETNP (Chenillat et al., 2012)

7.2. Role of local vs large scale circulation

In order to disentangle the changes of the local forcing related to upwelling, and the remote forcing (trade winds) on the eastern Pacific Ocean oxygen levels and productivity, we perform 2 supplementary experiments, PDO_MINUS50 and PDO_PLUS50. These experiments are similar to PDO_MINUS and PDO_PLUS. However, where oxygen is, anywhere in the water column, lower than 50 $mmol.m^{-3}$ at the end of the spinup (green line in the figures 7a-c), the MEAN surface forcing is employed (see 2 – "forcing and experiments"). As the resolution of the CORE forcing is relatively coarse (1.9°) and the NEMO circulation model interpolates the forcing on the ocean grid, we did not perform any explicit smoothing between the region where the MEAN and the PDO_MINUS / PDO_PLUS forcing are used.

The PDO_PLUS50 - PDO_MINUS50 SSH anomaly (Fig. 7a) presents a pattern similar to PDO_PLUS - PDO_MINUS SSH anomaly. The amplitude of PDO_PLUS50 - PDO_MINUS50 is however weaker than the amplitude of PDO_PLUS-PDO_MINUS in the eastern part of the Pacific basin (east of the green line – Fig 7a), showing that both remote and local forcings control the circulation properties east of 130°W in the equatorial region. This is consistent with the results of Zhang and McPhaden (2008) who showed that both the large scale circulation and the local wind stress anomalies impact the surface temperature variability in the NINO3 (150°W-90°; 5°N-5°S) region.

The PDO_PLUS50 – PDO_MINUS50 productivity anomaly (Fig 7b) and the PDO_PLUS-PDO_MINUS productivity anomaly displays a similar pattern in the western part of the basin. However, in the eastern part (east of the green line), the productivity is nearly identical in PDO_PLUS50 and PDO_MINUS50 suggesting that the change in productivity in the SUB20 regions is mostly driven by local forcings. The nutrients are indeed supplied into the euphotic zone by the upwelling systems, which are primarly driven by alongshore wind stress and curl (e.g Albert et al., 2010; Belmadani et al., 2014).

The oxygen concentration depends on both the changes in circulation and in productivity. In the eastern part of the basin (east of the green line), the PDO_PLUS50 - PDO_MINUS50 oxygen anomaly is similar to the PDO_PLUS – PDO_MINUS oxygen anomaly in the equatorial and southern part of SUB20 : a change in local forcings has nearly no impact on the simulated oxygen fields. These experiments suggest that the changes in oxygen concentration related to the change from a negative to a positive PDO phase are not directly related to changes in the coastal productivity and in the upwelling strength, but rather to changes in the large scale circulation in the equatorial and southern part of SUB20. Conversely, in the northern part of SUB20, local forcings play a dominant role as the PDO_PLUS50 – PDO_MINUS50 oxygen anomaly is positive while the PDO_PLUS – PDO_MINUS anomaly is negative.

8. Summary of the processes at play and conclusion

We tested here whether the PDO impacts the oxygen concentration in the eastern part of the Pacific Ocean. We use the forced ocean model NEMO coupled to a simple NPZD model. After spinup, the model NEMO-NPZD has been forced by "typical" PDO positive (experiment PDO_PLUS) and negative (experiment PDO_MINUS) conditions derived from the COREv2 atmospheric forcings. A PDO-positive phase is characterized by a decrease of the zonal and meridional wind speed over the Pacific Ocean by about 5% to 10 %, while the sea surface temperature increases by 0.2°C. A PDO-negative event shows the opposite pattern. In agreement with observations (McPhaden and Zhang, 2003), the

circulation of the tropical Pacific Ocean is more sluggish in the experiment PDO_PLUS compared to the experiment PDO_MINUS by 5 to 10 %. After 50 years of integration, the volume of the suboxic regions (oxygen lower then 20 $mmol.m^{-3}$) is larger by 7 % and the oxygen concentration decreases by 5 to 50 % in the suboxic regions in PDO_PLUS compared to PDO_MINUS.

Recent analyses of the observational datasets showed that the oxygen concentration decreased by about 5 % in the eastern equatorial Pacific Ocean region since 1960 (Schmidtko et al., 2017; Ito et al., 2017). We show here that a PDO_PLUS PDO event lasting for 50 years may impact the suboxic region by at least a similar order of magnitude. The shift to a PDO-negative phase (prevailing conditions before 1975) to a PDO positive phase (prevailing conditions since 1975) may therefore explain a significant percentage of the large deoxygenation that occurred during the last decades.

The simulated suboxic regions are divided into an equatorial (10°N-10°S), northern (10°N-30°N) and southern (10°S-30°S) part. The oxygen levels of each sub-region are constrained by different processes. In the equatorial part, the oxygen levels are set by advective processes (Cabre et al., 2015; Shigemitsu et al., 2017). In the PDO_PLUS experiment, the slowing-down of the equatorial current system (and more particularly of the equatorial undercurrent) decreases the supply of oxygen (Fig 8). Simultaneously, the supply of nutrients decreases, leading to a decrease in productivity and respiration. In the eastern part of the basin (in the suboxic regions), the decrease of supply dominates the change in respiration leading to a net oxygen decrease. Inversely, the change in respiration are dominant in the mid-Pacific Ocean, highlighting the importance of the parametrization of the biogeochemical processes (Kriest et al., 2010, Kriest and Oschlies, 2015) and more particularly the response of the phytoplankton growth to a change in nutrient concentration.

The southern part of the suboxic regions is mostly constrained by isopycnal diffusion processes (Gnanadesikan et al., 2012). In the PDO_PLUS experiment, the supply of oxygen by isopycnal processes from the equatorial regions and the subtropical gyres to the tropics decreases compared to PDO_MINUS. In the northern part, the role of diapycnal processes is dominant. In the experiment PDO_PLUS, the oxygen decrease is caused by changes in the upwelling system, stimulating productivity and respiration.

The general slow-down of the large-scale circulation caused by a decrease of the intensity of the trade winds is not reflected in the upwelling strength (Narayan et al., 2010), which is mainly forced by local processes. The strength and seasonality of the upwelling constrain the amount of productivity and the subsequent respiratiratory oxygen consumption in the suboxic regions. A shift in the upwelling seasonality explains the larger respiration in PDO_PLUS compared to PDO_MINUS in the northern part of the suboxic region. This shift is potentially linked to the NPGO (DiLorenzo et al., 2008), a decadal climate oscillation which signature is implicitly contained into the “typical” PDO forcing. Using 2 supplementary experiments where the PDO_PLUS and PDO_MINUS forcings are only applied in the mid Pacific Ocean above the tropical Pacific low-oygen areas, we highlighted that a change in the large scale wind pattern constrains changes in the equatorial and southern oxygen levels, while oxygen changes in the northern part is constrained by local processes.

One of the largest limitations of our study is that the idealized PDO forcings were prepared using a relatively short period extending from 1948 to 2007 (the COREv2 dataset). The implicit contribution of statistically independent climate oscillations such as the NPGO (DiLorenzo et al., 2008) can therefore not be completely ruled out.

Finally, another limitation is the resolution of the model. The role of the mesoscale activity has been previously demonstrated in the supply of oxygen to the suboxic regions of the eastern Pacific Ocean (Montes et al., 2014;

Bettencourt et al., 2015; Vergara et al., 2016). The relative increase of the isopycnal diffusive supply in a PDO-positive phase suggests an important role of the mesoscale activity.

Our study suggests that the shift from a prolongated (multidecadal) negative to a prolongated positive PDO phase is accompanied by a decrease in oxygen levels in the eastern tropical Pacific Ocean. Several multidecadal PDO shifts occurred in the last century. For instance, the period 1943-1976 is characterized by a negative PDO phase, while a positive PDO phase occurred from 1977 to 2011 (Fig 1a). Such shifts occurred almost every few decades during the last 1000 years, as shown by PDO reconstructions (MacDonald and Case, 2005). An open question is whether the succession of these alternate shifts may cause a change of the oxygen concentration on centennial to millennial time scales.

Our study can be compared to the study of Deutsch et al. (2011) (thereafter D2011). Based on a 1959-2005 hindcast experiment, D2011 showed that the global suboxic volume ($O2 < 5$ mmol.m-3), of which 95 % is contained in the north eastern tropical Pacific Ocean (0° to 30°N, 140°W to the coast), is controlled by the depth of the thermocline that constrains the productivity and the amount of oxygen respired around the suboxic volume. The depth of the thermocline is strongly related to the strength of the PDO, which explains 24 % of the variability of the suboxic volume in the hindcast simulation of D2011. In D2011, a PDO-negative phase was characterized by a large extent of the suboxic regions resulting from enhanced respiration with only negligible effects of changes in oxygen supply. Our results differ from D2011 because the increase of the respiration in a PDO-negative phase (higher primary production) is more than compensated by an increase in oxygen supply by advective / diffusive processes, leading ultimately to elevated oxygen levels and smaller suboxic regions in a PDO-negative state. Considering that the models used by D2011 and in our study are similar with similar grid resolution, the balance between changes in oxygen consumption (dominant effect in D2011) and transport (dominant effect in our study) depends on (i) the response of primary productivity and export production to a nutrient increase, and (ii) the depth of the suboxic regions, as respiration changes are stronger, and more difficult to compensate by oxygen supply changes, at shallower than at greater depths. While the biogeochemical model used in our study contains fully prognostic nutrient, phytoplankton, zooplankton and detritus fields, D2011 used a simple restoring model that diagnosed export production from restoring simulated against observed surface phosphate concentrations. Thereby, the model of D2011 did not account for possible PDO-driven changes in surface nutrient concentrations and instead likely overestimated the variability in export and respiration at depth.

While our modelling framework captures the general patterns of primary and export production reasonably well, it does not include an iron cycle and may thus, despite displaying a well-tuned mean state, exhibit systematic errors in the sensitivity to environmental changes. Furthermore, the model's representation of the respiration processes is relatively pragmatic. In particular, our model lacks an explicit nitrogen cycle including anaerobic remineralisation by denitrification under low oxygen conditions (Paulmier et al., 2009). Other limitations include for instance a simplistic parameterization of the attenuation of the flux of particulate organic matter that, in our model, neglects any dependence on temperature or oxygen (Laufkötter et al., 2017). Also not considered in the model is the diel vertical migration of zooplankton also actively transports material into the deep ocean (Bianchi et al., 2015). Anthropogenic activities impact the global biogeochemical cycles. In particular, atmospheric deposition of anthropogenic nitrogen and iron may partially relax the iron limitation in the tropical Pacific Ocean (Ito et al., 2016). Industrial fishing may affect the mortality rate of the zooplankton and possibly feed back on productivity and respiration (Getzlaff and Oschlies, 2017). Each of these 'missing' processes may modulate respiration rates and possibly being correlated with the state of the PDO. An important result of our study is that the PDO-induced changes in respiration are smaller than the PDO-induced changes in oxygen supply by a few percent in most of the eastern tropical Pacific Ocean. We show that this small

imbalance integrated over a few decades results in a significant PDO-driven oxygen anomaly that may explain a large part of the observed oxygen decline over the past decades in this region. Experiments including different biogeochemical parameterisations and processes will need to be performed to better assess the robustness of our results.

Bibliography

Albert, A., V. Echevin, M. L evy, and O. Aumont. Impact of nearshore wind stress curl on coastal circulation and primary productivity in the Peru upwelling system,J. Geophys. Res., 115, C12033, doi:10.1029/2010JC006569, 2010

Belmadani, A., V. Echevin, F. Codron, K. Takahashi, and C. Junquas. What dynamics drive future winds scenarios off Peru and Chile?, Clim. Dyn, 43 (7–8), 1893–1914, doi:10.1007/s00382-013-2015-2., 2014

Bettencourt, J.H., C. López, E. Hernández-Garcia, I. Montes, J. Sudre, B. Dewitte, A. Paulmier, and V. Garçon: Boundaries of the Peruvian Oxygen Minimum Zone shaped by coherent mesoscale dynamics, Nature Geoscience, doi:10.1038/ngeo2570, 2015

Bopp, L., Resplandy, L., Orr, J. C., Doney, S. C., Dunne, J. P., Gehlen, M., Halloran, P., Heinze, C., Ilyina, T., Séférian, R., Tjiputra, J., and Vichi, M: Multiple stressors of ocean ecosystems in the 21st century: Projections with CMIP5 models, Biogeosciences, 10, 6225–6245, doi:10.5194/bg-10-6225-2013, 2013

Bianchi, D., Galbraith, E.D., Carozza, D.A., Mislan, K.A.S., Stock, C.A. (2013) Intensification of open-ocean oxygen depletion by vertically migrating animals. *Nature Geoscience* 6, 545–548.

Brandt, P., Bange, H. W., Banyte, D., Dengler, M., Didwischus, S.-H., Fischer, T., Greatbatch, R. J., Hahn, J., Kanzow, T., Karstensen, J., Körtzinger, A., Krahmann, G., Schmidtko, S., Stramma, L., Tanhua, T., and Visbeck, M: On the role of circulation and mixing in the ventilation of oxygen minimum zones with a focus on the eastern tropical North Atlantic, Biogeosciences, 12, 489-512, https://doi.org/10.5194/bg-12-489-2015, 2015

Cabré, A., I. Marinov, R. Bernardello and D. Bianchi: Oxygen minimum zones in the tropical Pacific across CMIP5 models: mean state differences and climate change trends, Biogeosciences, 12, 5429-5454, doi:10.5194/bg-12-5429-2015, 2015

Chenillat, F., P. Rivière, X. Capet, E. Di Lorenzo, and B. Blanke: North Pacific Gyre Oscillation modulates seasonal timing and ecosystem functioning in the California Current upwelling system, Geophys. Res. Lett., 39, L01606, doi: 10.1029/2011GL49996, 2012

Cocco, V., Joos, F., Steinacher, M., Frölicher, T. L., Bopp, L., Dunne, J., Gehlen, M., Heinze, C., Orr, J., Oschlies, A., Schneider, B., Segschneider, J., and Tjiputra, J: Oxygen and indicators of stress for marine life in multi-model global warming projections, Biogeosciences, 10, 1849-1868, doi.org:10.5194/bg-10-1849-2013, 2013

Cravatte, S., G. Madec, T. Izumo, C. Menkes, and A. Bozec: Progress in the 3-D circulation of the eastern equatorial Pacific in a climate ocean model. Ocean Modell., 17, 28–48., 2007

Czeschel, R., L. Stramma, and G. C. Johnson: Oxygen decreases and variability in the eastern equatorial Pacific, J. Geophys. Res., 117, C11019, doi: 10.1029/2012JC008043, 2012

Deser, M. A. Alexander, and M. S. Timlin: Evidence for a wind-driven intensification of the Kuroshio current extension from the 1970s to the 1980s. J. Climate, 12, 1697–1706., 1999

Deutsch, C., H. Brix, T. Ito, H. Frenzel, and L. Thompson. Climate-forced variability of ocean hypoxia, Science, 333(6040), 336–339., 2011

Deutsch, C., W. Berelson, R. Thunell, T. Weber, C. Tems, J. McManus, J. Crusius, T. Ito, T. Baumgartner, V. Ferreira, J. Mey, and A. van Geen: Centennial changes in North Pacific anoxia linked to tropical trade winds, Science, 345(6197), 665–668, 2014

Di Lorenzo, E., N. Schneider , K.M. Cobb, J. S. Franks, K. Chhak, A. J. Miller, J. C. McWilliams , S. J. Bograd, H. Arango, E. Curchitser, T. M. Powell, P. Rivière: North Pacific Gyre Oscillation links ocean climate and ecosystem change: Geophys. Res. Lett., 35, L08607, doi:10.1029/2007GL032838, 2008

Dufresne, J-L., and 46 coauthors: Climate change projections using the IPSL-CM5 Earth System Model: from CMIP3 to CMIP5." Climate Dynamics 40.9-10: 2123-2165, 2013

Duteil, O., C. W. Böning, and A. Oschlies: Variability in subtropical-tropical cells drives oxygen levels in the tropical Pacific Ocean, Geophys. Res. Lett., 41, 8926–8934, doi:10.1002/2014GL061774, 2014a

Duteil, O., F. U. Schwarzkopf, C. W. Böning, and A. Oschlies: Major role of the equatorial current system in setting oxygen levels in the eastern tropical Atlantic Ocean: A high-resolution model study, Geophys. Res. Lett., 41, 2033–2040, doi:10.1002/2013GL058888., 2014b

Eddebbar, Y. A., M. C. Long, L. Resplandy, C. Rödenbeck, K. B. Rodgers, M. Manizza, and R. F. Keeling: Impacts of ENSO on air-sea oxygen exchange: Observations and mechanisms, Global Biogeochem. Cycles, 31, 901–921, doi:10.1002/2017GB005630., 2017

Garcia, H. E., R. A. Locarnini, T. P. Boyer, J. I. Antonov, O. K. Baranova, M. M. Zweng, and D. R. Johnson: World Ocean Atlas 2009, Volume 3: Dissolved oxygen, apparent oxygen utilization, and oxygen saturation, Ed. NOAA Atlas NESDIS 70, 344 pp., 2010

Getzlaff, J., and H. Dietze: Effects of increased isopycnal diffusivity mimicking the unresolved equatorial intermediate current system in an Earth system climate model, Geophys. Res. Lett., 40, 2166–2170, doi:10.1002/grl.50419., 2013

Getzlaff, J., H. Dietze, and A. Oschlies: Simulated effects of southern hemispheric wind changes on the Pacific oxygen minimum zone, Geophys. Res. Lett., 43, 728–734, doi:10.1002/2015GL066841., 2016

Getzlaff, J. und Oschlies, A. : Pilot Study on Potential Impacts of Fisheries-Induced Changes in Zooplankton Mortality on Marine Biogeochemistry. Global Biogeochemical Cycles, 31 (11). pp. 1656-1673. DOI 10.1002/2017GB005721, 2017

Gnanadesikan, A., J. P. Dunne, and J. John: Understanding why the volume of suboxic waters does not increase over centuries of global warming in an Earth System Model, Biogeosciences, 9, 1159–1172, 2012

Hong, L., L. Zhang, Z. Chen, and L. Wu: Linkage between the Pacific Decadal Oscillation and the low frequency variability of the Pacific Subtropical Cell, J. Geophys. Res. Oceans, 119, 3464–3477, doi:10.1002/2013JC009650, 2014

Ito, T., and C. Deutsch, A conceptual model for the temporal spectrum of oceanic oxygen variability, Geophys. Res. Lett., 37, L03601, doi: 10.1029/2009GL041595, 2010

Ito, T., and C. Deutsch: Variability of the oxygen minimum zone in the tropical North Pacific during the late twentieth century, Global Biogeochem. Cycles, 27, 1119–1128, doi:10.1002/2013GB004567, 2013

Ito T., A. Nenes, M. Johnson, N. Meskhidze and C. Deutsch: Acceleration of oxygen decline in the tropical Pacific over the past decades by aerosol pollutants, Nature Geosciences, doi:10.1038/ngeo2717, 2016

Ito, T., S. Minobe, M. C. Long, and C. Deutsch: Upper ocean O2 trends: 1958–2015, Geophys. Res. Lett., 44, 4214–4223, doi:10.1002/2017GL073613., 2017

Jiang, H., Q. Jin, H, Wang, R. Huang: Indices of strength and location for the North Pacific Subtropical and Subpolar Gyres. doi:10.1007/s13131-013-0310-8, 2013

Karnauskas, K. B., G. C. Johnson, and R. Murtugudde: An equatorial ocean bottleneck in global climate models, J. Clim., 25(1), 343–349, 2012

Karstensen, J., L. Stramm, and M. Visbeck: Oxygen minimum zones in the eastern tropical Atlantic and Pacific Oceans, Prog. Oceanogr., 77, 331–350, doi:10.1016/j.pocean.2007.05.009., 2008

Keller, D. P., I. Kriest, W. Koeve, and A. Oschlies: Southern Ocean biological impacts on global ocean oxygen, Geophys. Res. Lett., 43, 6469–6477, doi:10.1002/2016GL069630., 2016

Kriest, I., S. Khatiwala, and A. Oschlies: Towards an assessment of simple global marine biogeochemical models of different complexity, Prog. Oceanogr., 86(3–4), 337–360, doi:10.1016/j.pocean.2010.05.002., 2010

Kriest, I. und Oschlies, A. MOPS-1.0: modelling the regulation of the global oceanic nitrogen budget by marine biogeochemical processes. Geoscientific Model Development, 2929-2957. DOI 10.5194/gmd-8-2929-2015., 2015

Large, W. G., and S. G. Yeager: The global climatology of an interannually varying air-sea flux data set, Clim. Dyn., 33(2), 341–364., 2009

Laufkötter, C., J. G. John, C. A. Stock, and J. P. Dunne: Temperature and oxygen dependence of the remineralization of organic matter, *Global Biogeochem. Cycles*, 31, 1038–1050, doi:10.1002/2017GB005643, 2017

Lohmann, K., and M. Latif: Tropical Pacific decadal variability and the subtropical-tropical cells, J. Clim., 18, 5163–5177., 2005

Long, M. C., C. Deutsch, and T. Ito: Finding forced trends in oceanic oxygen, Global Biogeochem. Cycles, 30, 381–397, doi:10.1002/2015GB005310., 2016

Lübbecke, J. F., C. W. Böning, and A. Biastoch: Variability in the subtropical-tropical cells and its effect on near-surface temperature of the equatorial Pacific: A model study, Ocean Sci., 4, 529–569, doi:10.5194/osd-4-529-2007., 2008

Luo, Y., Q. Liu, and L. M. Rothstein: Increase of South Pacific eastern subtropical mode water under global warming, Geophys. Res. Lett., 38, L01601, doi: 10.1029/2010GL045878, 2011

Macias D, Landry MR, Gershunov A., Miller AJ, Franks PJS (2012) Climatic Control of Upwelling Variability along the Western North-American Coast. PLoS ONE7(1): e30436. doi:10.1371/journal.pone.0030436, 2012

Madec, G.: NEMO ocean engine version 3.1. Note Pole Modelisation. 27, Inst. Pierre-Simon Laplace, Paris., 2008

Mantua, N.J. and S.R. Hare, Y. Zhang, J.M. Wallace, and R.C. Francis: A Pacific interdecadal climate oscillation with impacts on salmon production. Bulletin of the American Meteorological Society, 78, pp. 1069-1079., 1997

Marin, F., E. Kestenare, T. Delcroix, F. Durand, S. Cravatte, G. Eldin, and R. Bourdalle-Badie: Annual reversal of the equatorial intermediate current in the Pacific: Observations and model diagnostics. J. Phys. Oceanogr., 40, 915–933, 2010

Matear, R. J., and A. C. Hirst: Long-term changes in dissolved oxygen concentrations in the ocean caused by protracted global warming, Global Biogeochem. Cycles, 17, 1125, doi:10.1029/2002GB001997, 4, 2003MacDonald, G. M., and R. A. Case: Variations in the Pacific Decadal Oscillation over the past millennium, Geophys. Res. Lett., 32, L08703, doi:10.1029/2005GL022478, 2005

McCreary, J. P., and P. Lu: On the interaction between the subtropical and equatorial ocean circulation: The Subtropical Cell, J. Phys. Oceanogr., 24, 466–497, 1994

McPhaden, M. J., and D. Zhang: Slowdown of the meridional overturning circulation in the upper Pacific Ocean, Nature, 415, 603–608, 2002

Merrifield, M. A., P. R. Thompson, and M. Lander: Multidecadal sea level anomalies and trends in the western tropical Pacific, Geophys.Res. Lett., 39, L13602, doi:10.1029/2012GL052032, 2012

Messié, M. and F. Chavez, Global Modes of Sea Surface Temperature Variability in Relation to Regional Climate Indices. J. Climate, 24, 4314–4331, https://doi.org/10.1175/2011JCLI3941.1, 2011

Miller, A.J., D.R. Cayan, T.P. Barnett, N.E. Graham and J.M. Oberhuber. The 1976-77 climate shift of the Pacific Ocean. Oceanography 7, 21-26, 1994

Montes, I., B. Dewitte, E. Gutknecht, A. Paulmier, I. Dadou, A. Oschlies, and V. Garçon. High-resolution modeling of the Eastern Tropical Pacific Oxygen Minimum Zone: Sensitivity to the tropical ocean circulation, J. Geophys. Res. Oceans, 119 (8), 5515 - 5532, doi:10.1002/2014JC009858, 2014

Narayan, N., Paul, A., Mulitza, S., and Schulz, M: Trends in coastal upwelling intensity during the late 20th century, Ocean Sci., 6, 815-823, doi:10.5194/os-6-815-2010, 2010

Oschlies, A., Duteil, O., Getzlaff, J., Koeve, W., Landolfi, A. und Schmidtko, S. Patterns of deoxygenation: sensitivity to natural and anthropogenic drivers. Philosophical Transactions of the Royal Society A: Mathematical, Physical and Engineering Sciences, 375 (2102). p. 20160325. DOI 10.1098/rsta.2016.0325, 2017

Paulmier, A., Kriest, I., and Oschlies, A: Stoichiometries of remineralisation and denitrification in global biogeochemical ocean models, Biogeosciences, 6, 923-935, https://doi.org/10.5194/bg-6-923-2009, 2009

Qu, T., and J. Chen: A North Pacific decadal variability in subduction rate, Geophys. Res. Lett., 36, L22602, doi:10.1029/2009GL040914, 2009

Ridder, N. N., and M. H. England: Sensitivity of ocean oxygenation to variations in tropical zonal wind stress magnitude, Global Biogeochem. Cycles, 28, 909–926, doi:10.1002/2013GB004708, 2014

Schmidtko, S., L. Stramma und M. Visbeck: Decline in global oxygen content during the past five decades. Nature, doi:10.1038/nature21399, 2017

Shigemitsu, M., A. Yamamoto, A. Oka, and Y. Yamanaka: One possible uncertainty in CMIP5 projections of low-oxygen water volume in the Eastern Tropical Pacific, Global Biogeochem. Cycles, 31, 804–820, doi:10.1002/2016GB005447, 2017

Smith, T.M., R.W. Reynolds, T.C. Peterson, and J. Lawrimore: Improvements NOAAs Historical Merged Land–Ocean Temp Analysis (1880–2006). Journal of Climate, 21, 2283–2296, 2008.

Stramma, L., G. C. Johnson, J. Sprintall, and V. Mohrholz: Expanding oxygen-minimum zones in the tropical oceans, Science, 320, 655–658, 2008

Stramma, L., Johnson, G. C., Firing, E., and Schmidtko, S: Eastern Pacific oxygen minimum zones: Supply paths and multidecadal changes, J. Geophys. Res.-Oceans, 115, C09011, doi:10.1029/2009jc005976, 2010

Stramma, L., A. Oschlies, and S. Schmidtko: Mismatch between observed and modeled trends in dissolved upper-ocean oxygen over the last 50 yr, Biogeosciences, 9, 4045–4057, doi:10.5194/bg-9-4045-2012, 2012

Thomas, A.C., P. T. Strub, R.A Waetherbee, C. James: Satellite views of Pacific chlorophyll variability: Comparisons to physical variability, local versus nonlocal influences and links to climate indices. Deep-Sea Res. II, doi:10.1016/j.dsr2.2012.04.008, 2012

Vergara, O., B. Dewitte, I. Montes, V. Garçon, M. Ramos, A. Paulmier, and O. Pizarro: Seasonal Variability of the Oxygen Minimum Zone off Peru in a high-resolution regional coupled model. Biogeosciences, 13, 4389-4410. Doi:10.5194/bg-13-4389-2016, 2016

Yamamoto, A., A. Abe-Ouchi, M. Shigemitsu, A. Oka, K. Takahashi, R. Ohgaito, and Y. Yamanaka: Global deep ocean oxygenation by enhanced ventilation in the Southern Ocean under long-term global warming, Global Biogeochem. Cycles, 29, 1801–1815, doi:10.1002/2015GB005181., 2015

Yang, H., Liu, J., Lohmann, G., Shi, X. , Hu, Y. and Chen, X.: Ocean-atmosphere dynamics changes associated with prominent ocean surface turbulent heat fluxes trends during 1958–2013. Ocean Dynamics 66: 353. doi:10.1007/s10236-016-0925-3, 2016Zhang, X. and .J. McPhaden: Eastern Equatorial Pacific Forcing of ENSO Sea Surface Temperature Anomalies. J. Climate, 21, 6070–6079, https://doi.org/10.1175/2008JCLI2422.1, 2008

Zhang, L., and T. L. Delworth: Analysis of the characteristics and mechanisms of the Pacific decadal oscillation in a suite of coupled models from the Geophysical Fluid Dynamics Laboratory. J. Climate, 28, 7678–7701, doi: 10.1175/JCLI-D-14-00647.1, 2015

Zhou, X., Alves A., Marsland S.J., Daohua B., Hirst A.C: Multi-decadal variations of the South Indian Ocean subsurface temperature influenced by Pacific Decadal Oscillation, Tellus A: Dynamic Meteorology and Oceanography, 69:1, 1308055, DOI: 10.1080/16000870.2017.1308055, 2017

Figures

Figure 1 : a – Pacific Decadal Oscillation index (PDO) (annual averages 1900 - 2017) (data from the 'Joint Institute for the Study of the Atmosphere and Ocean – University of Washington, USA : http://research.jisao.washington.edu/data_sets/pdo). The period 1948 – 2007 has been highlighted. The contour line is the smoothed PDO index (20 years running mean). b – average of the zonal 10m wind component ($m.s^{-1}$) of the PDO positive (PDO_PLUS experiment) phase minus PDO negative phase (PDO_MINUS experiment). Contour : zonal wind component average ($m.s^{-1}$) 1948-2007. c – average of the meridional wind component($m.s^{-1}$) of the PDO positive phase (PDO_PLUS experiment) minus PDO negative phase (PDO_MINUS experiment). Contour : meridional wind component average ($m.s^{-1}$) 1948-2007. d – average of the 10m air temperature (°C) of the PDO positive phase (PDO_PLUS experiment) minus PDO negative phase (PDO_MINUS experiment). Contour : average of the 10m air temperature (°C) 1948-2007. e- difference between the barotropic streamfunction (BSf) PDO_PLUS and PDO_MINUS (Sv). Black contour: PDO_MINUS BSf, red contour: PDO_PLUS BSf. The sense of rotation is clockwise for positive values. f- difference between the Sea Surface Height (SSH) PDO_PLUS and PDO_MINUS (m). black contour : SSH PDO_MINUS. Red contour : SSH PDO_PLUS. g- difference between the meridional overturning (MOC) PDO_PLUS – PDO_MINUS (Sv). black contour : MOC PDO_MINUS. Red contour : MOC PDO_PLUS. The sense of rotation is clockwise for positive values. All the differences between PDO_PLUS and PDO_MINUS are averaged over 50 years of integration.

Figure 2 : a – oxygen concentration ($mmol.m^{-3}$) at the end of the spinup (average 100-700m). Contour : oxygen concentration of the World Ocean Atlas (WOA) ($mmol.m^{-3}$) (average 100-700m). b – thickness (m) of the suboxic regions (oxygen lower than 20 $mmol.m^{-3}$) in WOA and -c at the end of the spinup. d – difference in percentage between the oxygen concentration in PDO_PLUS and in PDO_MINUS (average 100-700 m). Black contour : oxygen concentration PDO_MINUS. Red contour : oxygen concentration in PDO_PLUS ($mmol.m^{-3}$). e – difference between the oxygen concentration ($mmol.m^{-3}$) in PDO_PLUS and in PDO_MINUS vertically averaged over the suboxic regions SUB20 (defined as the region where the oxygen concentration is lower than 20 $mmol.m^{-3}$ at the end of the spinup). Contour : difference between the oxygen concentrations ($mmol.m^{-3}$) in PDO_PLUS and PDO_MINUS (average 100-700m). f – difference between the thickness (m) of the suboxic regions in PDO_PLUS and PDO_MINUS. All the differences between PDO_PLUS and PDO_MINUS are averaged after 50 years of integration.

Figure 3 : budget of the oxygen concentration (average 100m-700m) ($mmol.m^{-3}.yr^{-1}$) at the end of the spinup (a-d) and difference between PDO_PLUS and PDO_MINUS averaged over 50 years of integration (e-f). a,e : respiration. b,f: total supply. c,g : advective processes. d,h: diffusive processes. The oxygen concentration ($mmol.m^{-3}$) is displayed in contour in a-d. The oxygen difference between PDO_PLUS and PDO_MINUS ($mmol.m^{-3}$) is displayed in contour in e-f. As a note of caution, a positive value corresponds to a source of oxygen while a negative value corresponds to a sink in a-d, while differences between two experiments are displayed in e-f.

Figure 4 : a – zonal integration of the vertically averaged oxygen supply in the suboxic regions SUB20 (oxygen lower than 20 mmol.m-3) ($mmol.m^{-2}.yr^{-1}$) at the end of the spinup. Black : total supply. Red : advective processes. Blue: isopycnal diffusion. Green : diapycnal diffusion. b – relative importance of the advective processes (red), isopycnal diffusion (blue) and diapycnal diffusion (green) in the total oxygen supply in SUB20 (Plain : PDO_MINUS experiment, dashed : PDO_PLUS experiment). c – zonal integration of the vertically averaged difference of oxygen supply/removal in PDO_PLUS minus PDO_MINUS($mmol.m^{-2}.yr^{-1}$) in SUB20. Black: supply. Green: respiration. Red: supply + respiration. d – zonal integration of the vertically averaged difference of oxygen supply in PDO_PLUS minus

PDO_MINUS(mmol.$m^{-2.}$ yr^{-1}) in SUB20. Black : total supply. Red: advective processes. Blue: isopycnal diffusion. Green : diapycnal diffusion.

Figure 5: a – timeseries (50 years) of the difference between PDO_PLUS and PDO_MINUS of the oxygen concentration (mmol.m^{-3}) in the region EQ (average 10°N-10°S, 160°E-140°W, 100-700m) (black), SUB20EQ (equatorial part of SUB20: 10°S-10°N) (deep blue), SUB20N (northern part of SUB20: 10°N-30°N) (light blue), SUB20S (southern part of SUB20: 10°S-30°S) (purple). b,c,d : oxygen (mmol.m^{-3}) difference (average 100-700 m) between PDO_PLUS an PDO_MINUS after b -2 years, c- 10 years, d- 20 years of integration. e-h: timeserie (50 years) of the difference between the PDO_PLUS and PDO_MINUS oxygen budget (mmol.m^{-3}.yr^{-1}) in e-EQ, f-SUB20EQ, g-SUB20N,h-SUB20S. Bold black : total supply. Blue : advective supply. Pink: diapycnal diffusion. Light blue : dia. + isopycnal diffusion. Bold green : respiration. Bold red: supply + respiration

Figure 6: a - difference (%) of the vertically integrated phytoplankton concentration between PDO_PLUS and PDO_MINUS (average of 50 years integration). The vertically integrated phytoplankton concentration of PDO_MINUS is shown in contour (mmol.m^{-2}). b - difference (%) of the surface phosphate concentration between PDO_PLUS and PDO_MINUS (average of 50 years integration). The surface phosphate concentration of PDO_MINUS is shown in contour (mmol.m^{-2}). c,e,g: average region 10°S-20°S/90°W-60°W and d,f,h region 10°N:20°N/120°W-90°W. c,d: upwelling (m.yr^{-1}) (blue : PDO_MINUS, red: PDO_PLUS). e,f : phytoplankton concentration (mmol.m^{-3}) (contour : phosphate concentration: mmol.m^{-3}) at the end of the spinup. g,h : difference betweee PDO_PLUS and PDO_MINUS in phytoplankton concentration (mmol.m^{-3}) (contour : difference between PDO_MINUS and PDO_PLUS in phosphate concentration: mmol.m^{-3})

Figure 7: a – difference between the sea surface height (m) of the experiment PDO_PLUS50 and PDO_MINUS50 (colors) and PDO_PLUS and PDO_MINUS (contour). b – difference between the vertically integrated phytoplankton concentration (mmol.m^{-2}) of the experiment PDO_PLUS50 and PDO_MINUS50 (color) and PDO_PLUS and PDO_MINUS (contour). c- difference between the average 100m – 700m oxygen concentration (mmol.m^{-3}) of the experiment PDO_PLUS50 and PDO_MINUS50 (color) and PDO_PLUS and PDO_MINUS (contour).

Figure 8 : summary of the processes at play during a PDO positive (red) and negative phase (blue).

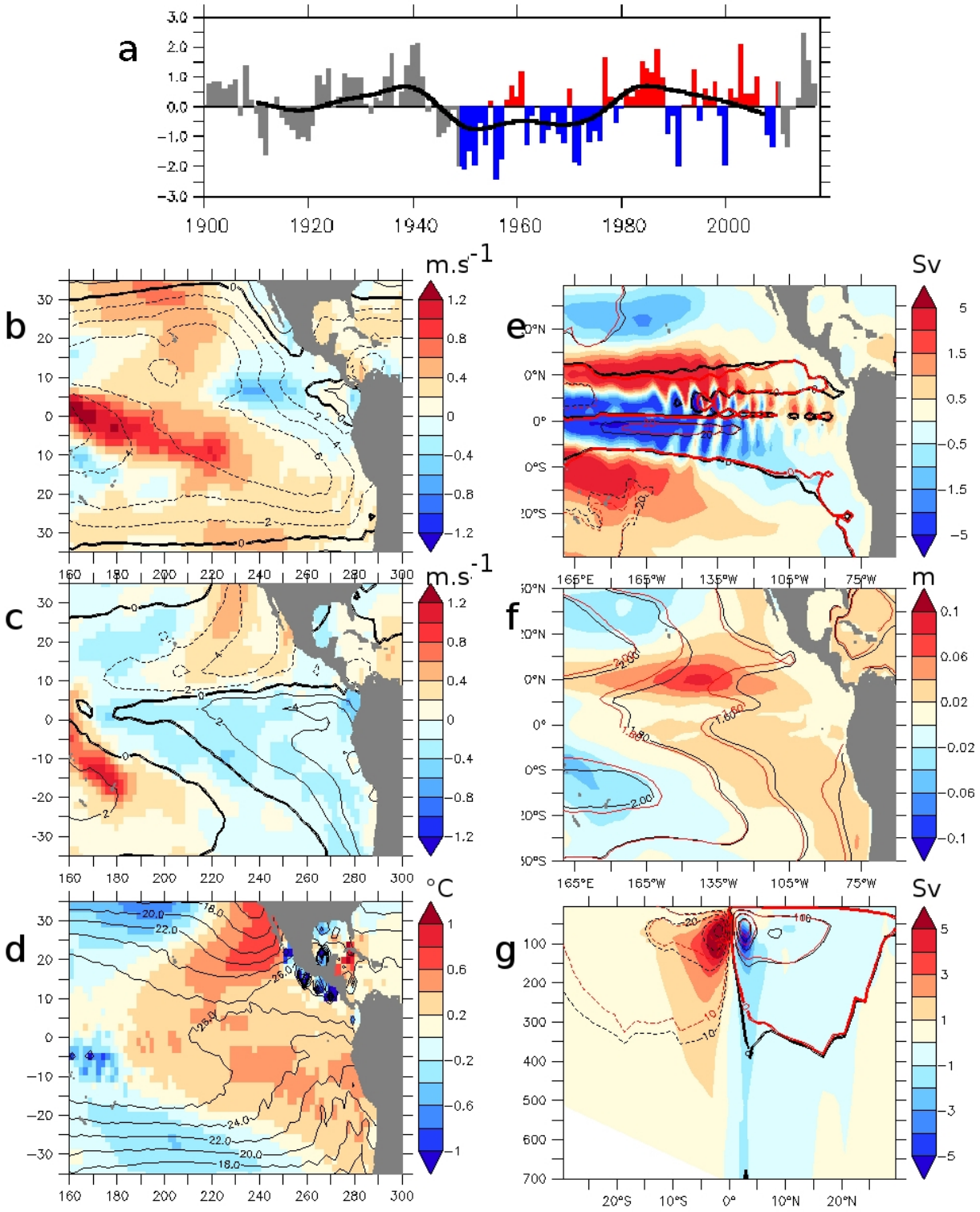

Figure 1

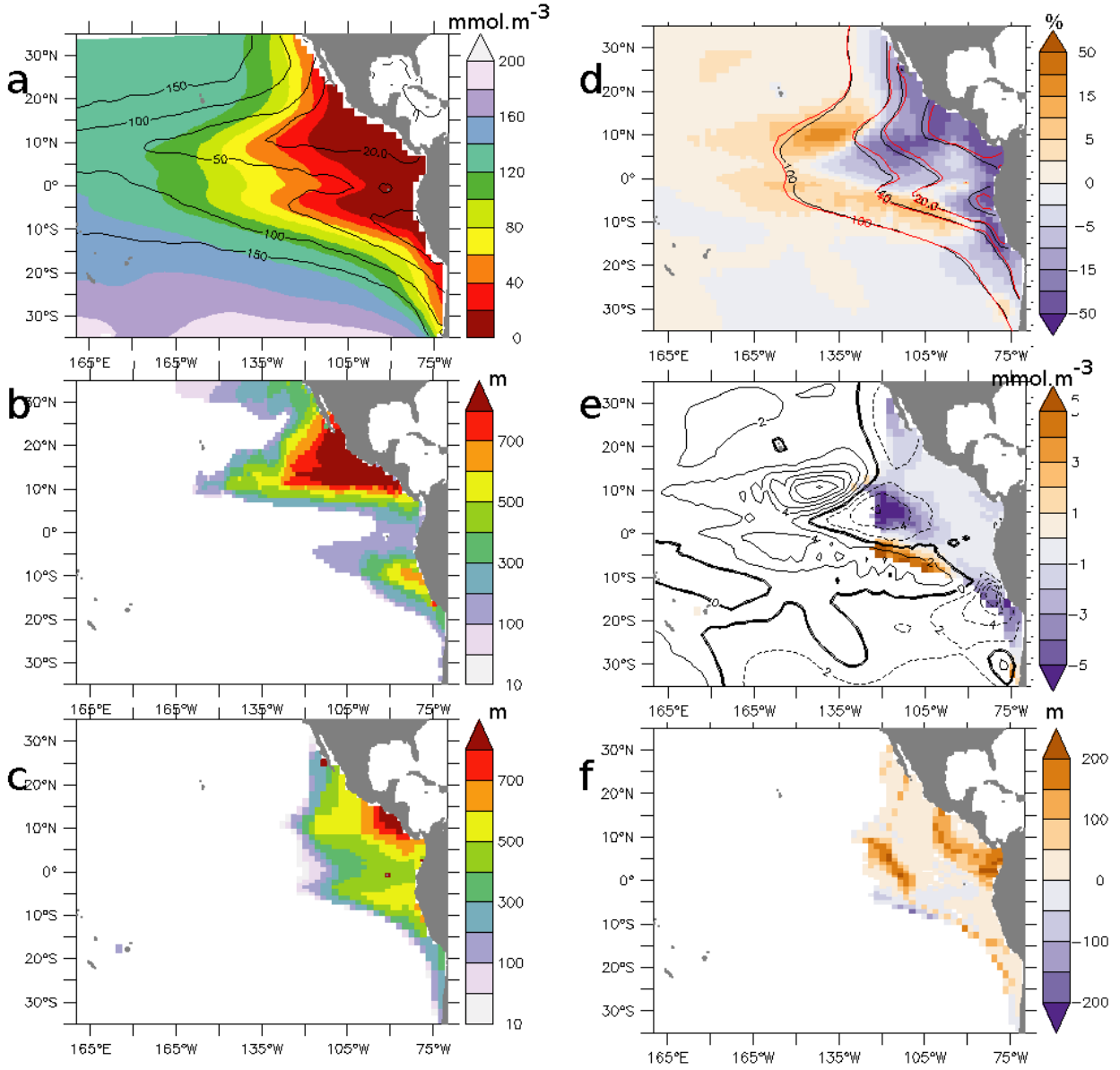
a
b
c
d
e
f
mmol.m-3
m
%
30°N
20°N
10°N
0°
10°S
20°S
30°S
165°E
165°W
135°W
105°W
75°W
150
100
50
20.0
200
160
120
80
40
0
700
500
300
100
10
50
15
5
0
−5
−15
−50
2
4
3
1
−1
−3
−5
200
100
0
−100
−200

Figure 2

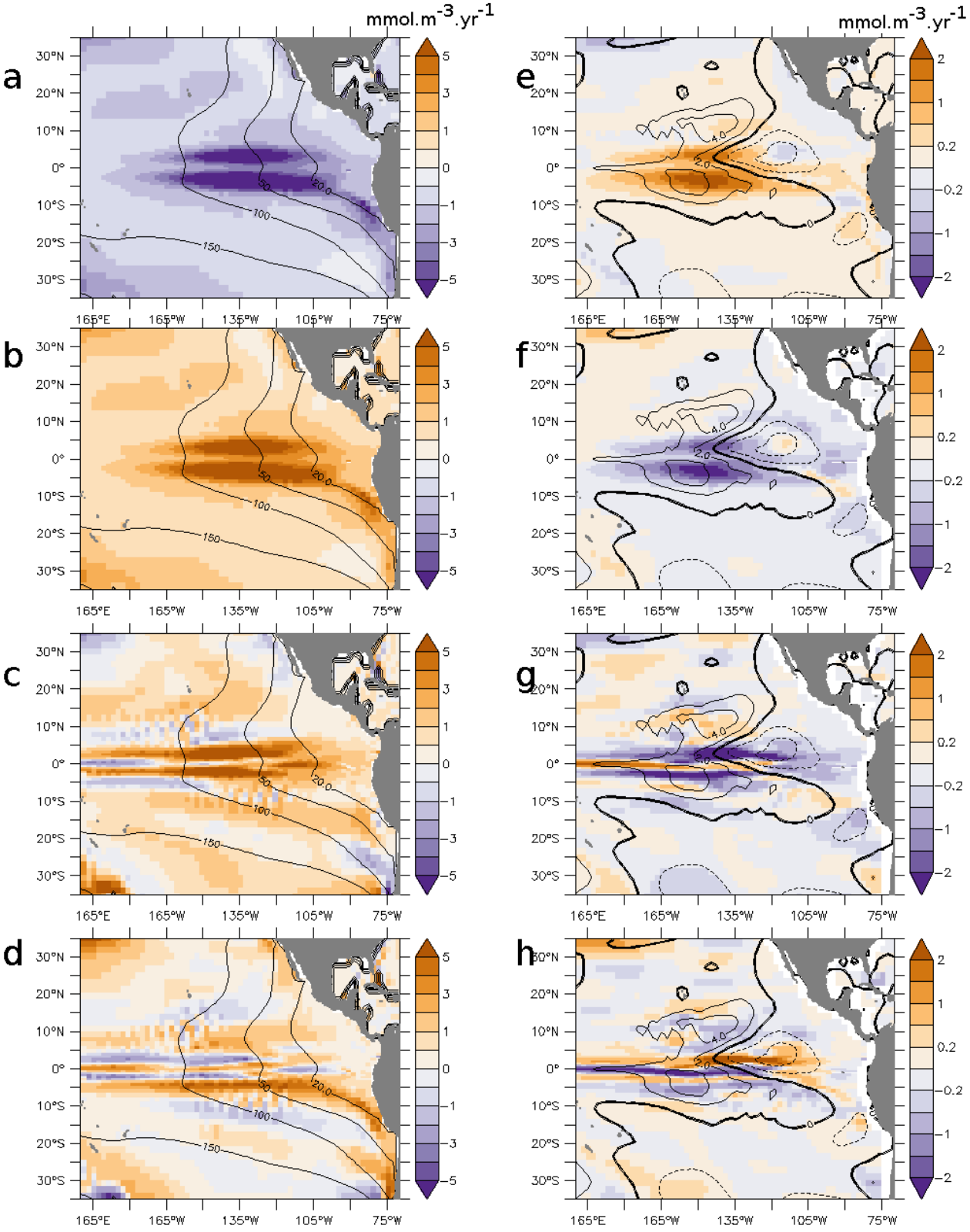
a
b
c
d
e
f
g
h
mmol.m-3.yr-1
mmol.m-3.yr-1
30°N
20°N
10°N
0°
10°S
20°S
30°S
165°E
165°W
135°W
105°W
75°W
5
3
1
0
-1
-3
-5
2
1
0.2
-0.2
-1
-2
50
20.0
100
150
4.0
2.0
0

Figure 3

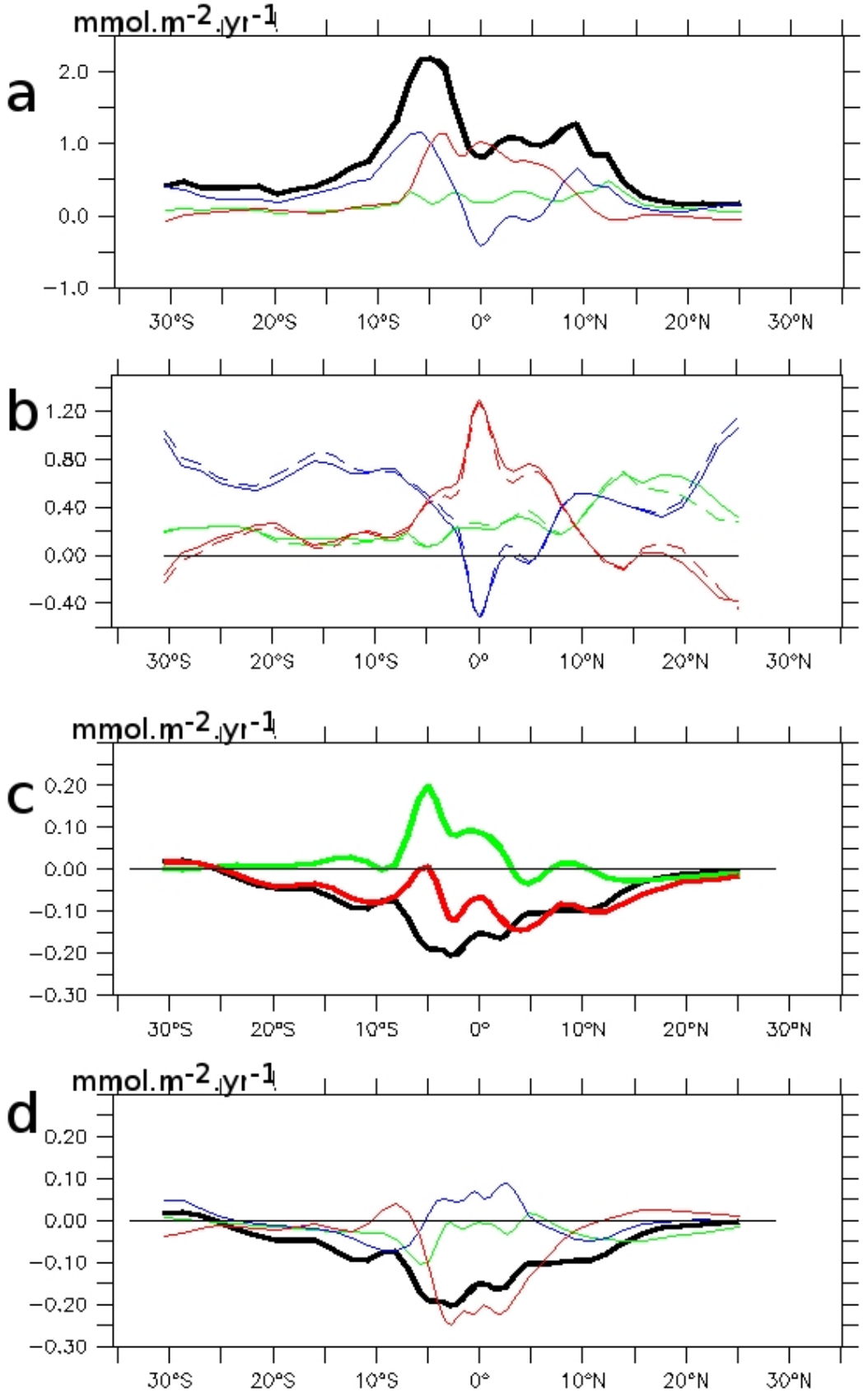
a
mmol.m-2.yr-1
2.0
1.0
0.0
−1.0
30°S
20°S
10°S
0°
10°N
20°N
30°N
b
1.20
0.80
0.40
0.00
−0.40
30°S
20°S
10°S
0°
10°N
20°N
30°N
c
mmol.m-2.yr-1
0.20
0.10
0.00
−0.10
−0.20
−0.30
30°S
20°S
10°S
0°
10°N
20°N
30°N
d
mmol.m-2.yr-1
0.20
0.10
0.00
−0.10
−0.20
−0.30
30°S
20°S
10°S
0°
10°N
20°N
30°N

Figure 4

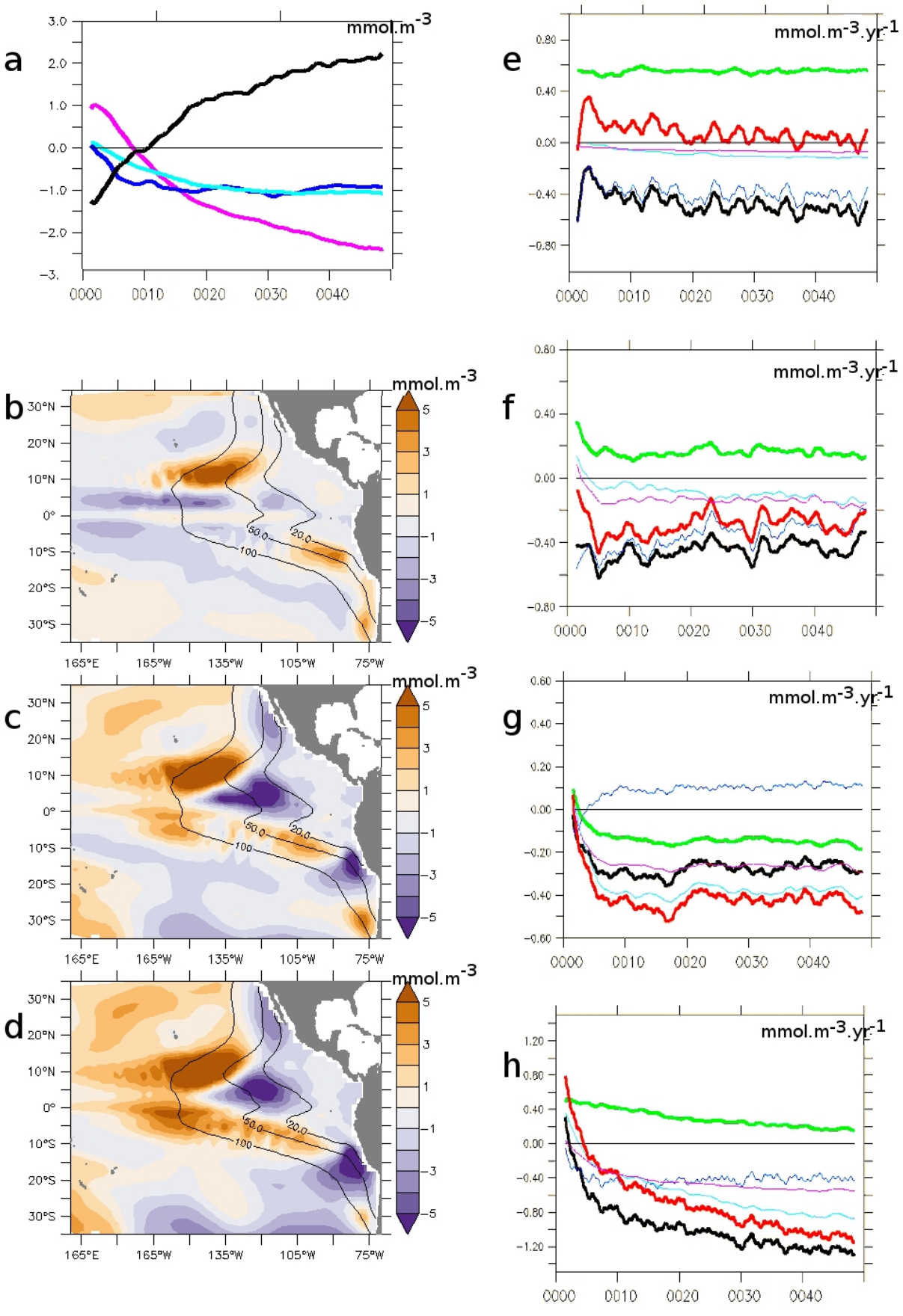
a
mmol.m-3
3.0
2.0
1.0
0.0
−1.0
−2.0
−3.
0000
0010
0020
0030
0040
b
mmol.m-3
30°N
20°N
10°N
0°
10°S
20°S
30°S
165°E
165°W
135°W
105°W
75°W
50.0
20.0
100
5
3
1
−1
−3
−5
c
mmol.m-3
d
mmol.m-3
e
mmol.m-3.yr-1
0.80
0.40
0.00
−0.40
−0.80
f
mmol.m-3.yr-1
g
mmol.m-3.yr-1
0.60
0.40
0.20
0.00
−0.20
−0.40
−0.60
h
mmol.m-3.yr-1
1.20
0.80
0.40
0.00
−0.40
−0.80
−1.20

Figure 5

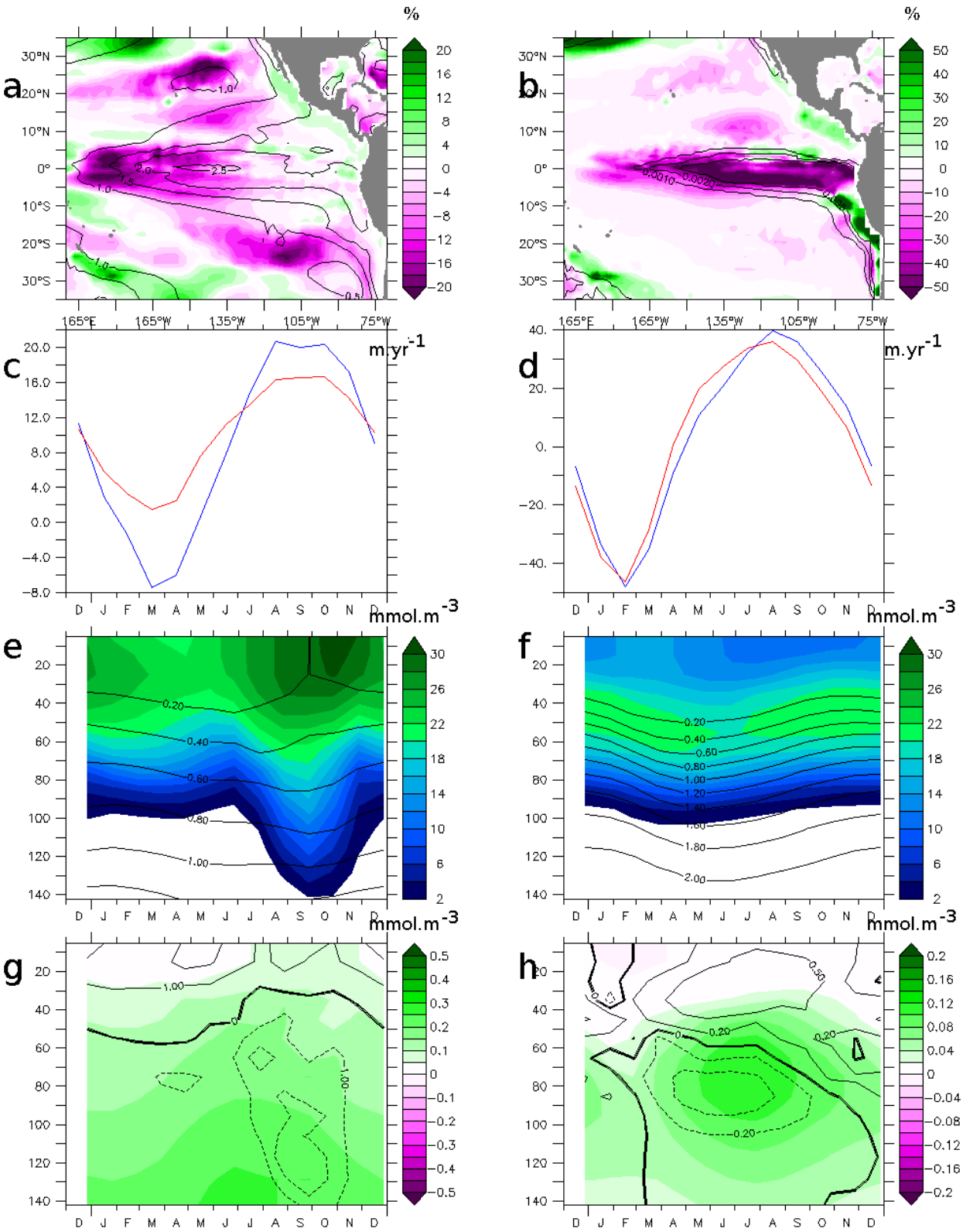
a
b
c
d
e
f
g
h
%
m.yr-1
mmol.m-3
30°N
20°N
10°N
0°
10°S
20°S
30°S
165°E
165°W
135°W
105°W
75°W
D J F M A M J J A S O N D

Figure 6

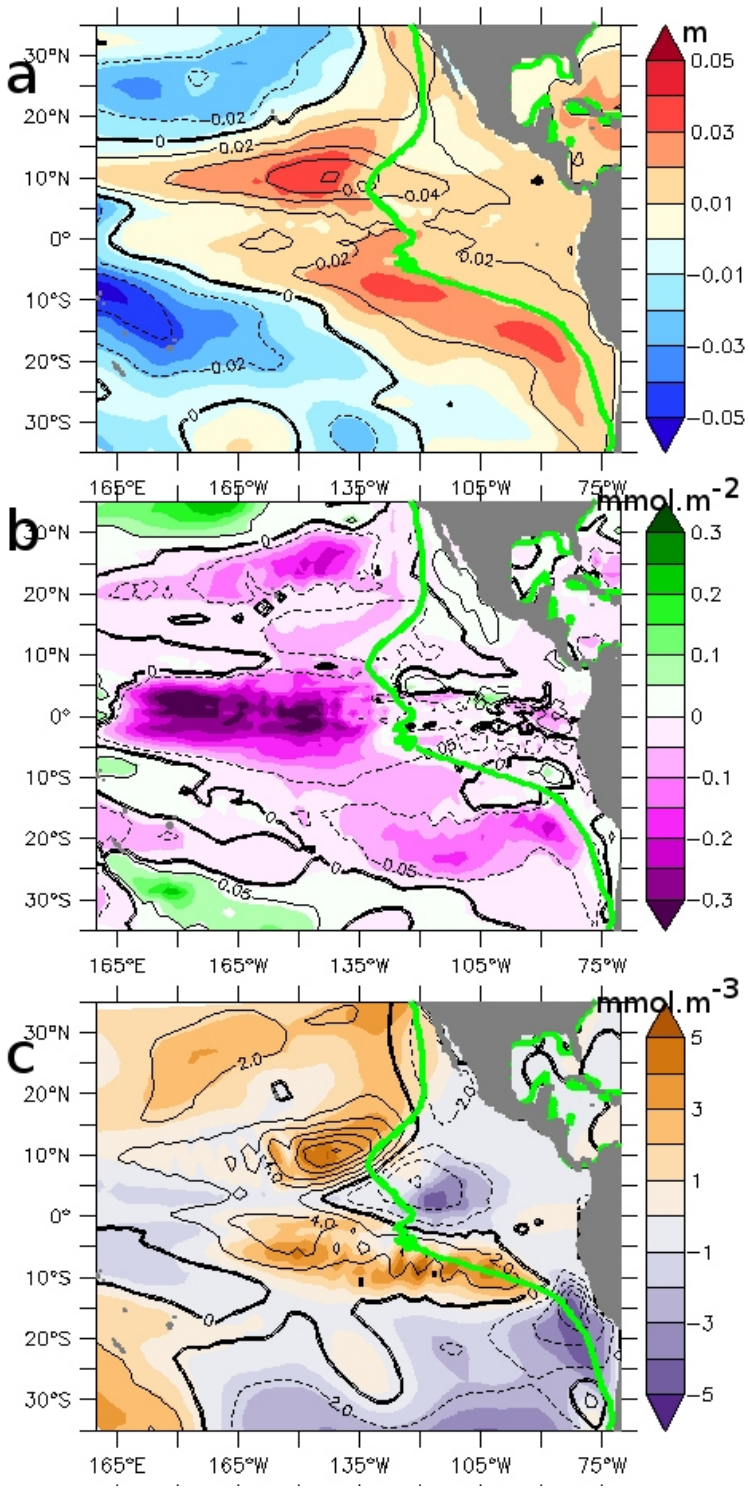
a
m
0.05
0.03
0.01
−0.01
−0.03
−0.05
b
mmol.m-2
0.3
0.2
0.1
0
−0.1
−0.2
−0.3
c
mmol.m-3
5
3
1
−1
−3
−5
30°N
20°N
10°N
0°
10°S
20°S
30°S
165°E
165°W
135°W
105°W
75°W

Figure 7

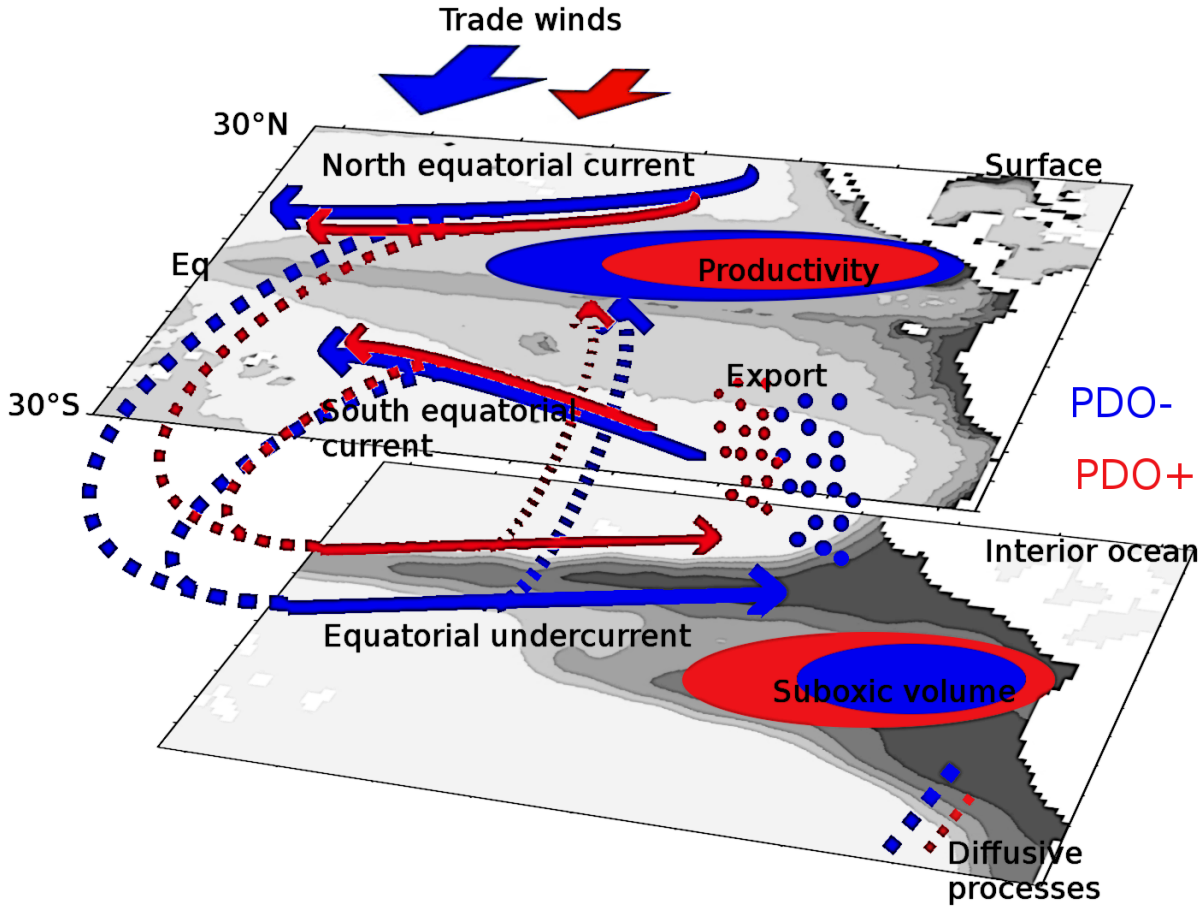
Trade winds
30°N
North equatorial current
Surface
Eq
Productivity
Export
30°S
South equatorial current
PDO-
PDO+
Interior ocean
Equatorial undercurrent
Suboxic volume
Diffusive processes

Figure 8